Cyclic Behavior of Timber Column Concealed Base Joint[*1]

Jérôme Humbert[*2†], Sang-Joon Lee[*2], Joo-Saeng Park[*2], Moon-Jae Park[*2]

ABSTRACT

This paper presents experimental and numerical tests on a recently developed timber column concealed base joint. This joint was designed to replace the wood-wood connection found in the post-and-beam structure of *Hanok*, the traditional Korean timber house. The use of metallic connectors provides an increased ductility and energy dissipation for a better performance under reversed loading, especially seismic. In this study, we investigate the performance of the joint under pseudo-static reversed cyclic moment loading through the study of its ductility and energy dissipation. We first perform experimental tests. Results show that the failure occurs in the metallic connector itself because of stress concentrations, while no brittle fracture of wood occur. Subsequent numerical simulations using a refined finite element model confirm these conclusions. Then, using a practical modification of the joint configuration with limited visual impact, we improve the ductility and energy dissipation of the joint while retaining a same level of rotational strength as the originally designed configuration. We conclude that the joint has a satisfying behavior under reversed moment loading for use in earthquake resistant timber structure in low to moderate seismicity areas like Korea.

Keywords : timber structure, concealed joint, post-and-beam, metallic connector, cyclic test, moment resistance

1. INTRODUCTION

Hanok, the traditional Korean timber house, remains fairly popular despite limited performances in terms of e. g. structural resistance or thermal insulation. In the context of an effort to modernize the *Hanok* house while preserving its visual identity, Korea Forest Research Institute (KFRI) is developing a hybrid design of timber house based on the traditional post-and-beam structure of *Hanok.* This ongoing 4-year research also aims at developing higher multi-story timber structures by use of engineered timber products like *e.g.* glued laminated timber *(Glulam).* This project includes several experimental and numerical tests at different scales on timber joints,

Jérôme Humbert, Sang-Joon Lee, Joo-Saeng Park, Moon-Jae Park
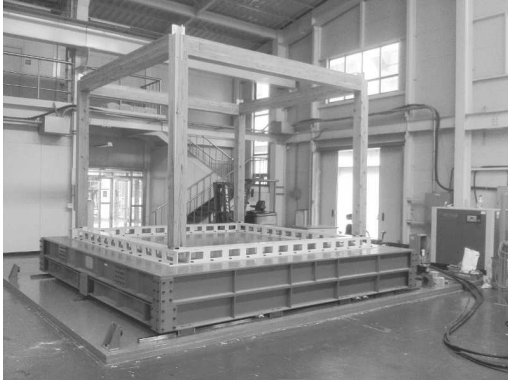
Fig. 1. Shaking table with sample timber frame made with the studied metallic joints.

Fig. 2. Column base slotted-in connector with pin.

structural elements (walls), and full-scale two-story timber house specimens using a new shaking table installed at KFRI (Fig. 1).

The proposed hybrid design of timber house, focusing both on structural and thermal insulation performances, is composed first of a post-and-beam structure for the vertical load. This structure is apparent, thereby retaining the visual identity of the *Hanok*. However, the lateral resistance of the post-and-beam structure alone is limited (see *e.g.* [1]). In the literature, several studies focused on improving the moment resistance of the timber joints[2-4] or the timber column themselves[5-7]. However Smith[8] notes that this is a difficult problem, especially for Glulam because of the brittle fracture of wood. Smith therefore suggests that bracing is the preferred method for lateral resistance. Thus, in order to improve the lateral resistance of the post-and-beam structure, modern wall technologies are used in complement. Two technologies are considered: light-frame shear walls, which provide a reference of lateral-resistant wall with well-known performance[9-11], and Structural Insulation Panels (SIP)[1], which provide at the same time a lateral resistance and an increased thermal insulation. Moreover, the traditional wood-wood connections of the post-and-beam struc-
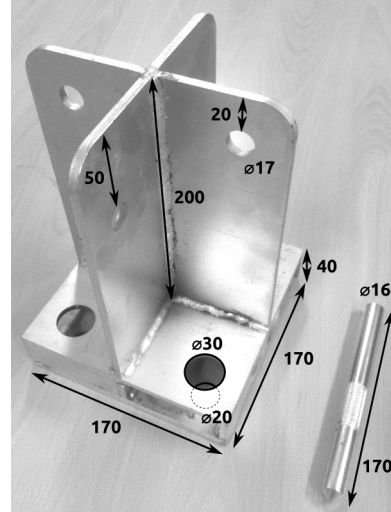
ture are replaced with joints with metallic connectors in order to increase the ductility and energy dissipation of the structure, thereby providing a better safety through a less sudden and more visually noticeable failure. In parallel, the need for a preserved visual identity calls for the use of concealed slotted-in metallic connectors. In this context, a new type of slotted-in metallic connector (Fig. 2) was developed at KFRI in some previous works[1,12]. Although some experimental tests at the shearwall scale ensured this system was well designed, the behavior under lateral reversed loading of the joint itself was left unclear.

As a consequence, we present in this paper experimental tests on this column base joint under pseudo-static reversed cyclic loadings. The tests results are aimed at assessing the cyclic and seismic performance of the connector through the study of its ductility and energy dissipation. Indeed, in a structure undergoing a lateral loading (*e.g.* wind or earthquake), the anchorage connections at the wall extremities are subject to both a vertical uplift and a moment loading. Despite the use of complementary lateral-resis-

tant structural element, it is necessary to assess the resistance of the timber column joint, and in particular the load transfer between the shear wall and the post-and-beam structure in the proposed hybrid design. In the following, this first work focuses on the moment-carrying capacity of the joint. The study of the tension resistance (uplift) is an ongoing work left for a future communication.

In parallel of the experimental tests, we also present complementary numerical simulations on a refined finite element (FE) model. This model is used here for validation at the structural element scale (connector scale), and will serve as a reference later to derive a macro-scale model at the structure scale (multi-story timber house scale) for obvious reasons of prohibitive simulation times. However, this refined model, once validated, can provide for the fitting of the macro-scale model complementary results not available from experimental tests. This multi-scale approach allows reduced experimental costs, and has been successfully applied in previous studies (see *e.g.* [9,13]).

In the following, we first present the experimental tests and results on the timber column joint under reversed cyclic moment loading. Then, we present the refined FE model and compare the numerical results with the experimental results. After that, we propose an improvement of the joint ductility through a practical modification of the connector configuration. We confirm this improvement through a second series of experimental tests. Finally, we give some conclusions of this work and perspectives for future studies.

2. MATERIALS and METHODS

The timber column joint considered in this study is presented in [1,12]. We recall its main characteristics for the sake of consistency. The joint is composed of a metallic connector slotted in the timber member, as seen on Fig. 1. The metallic connector itself (Fig. 2) is composed of a lower 170 mm × 170 mm square base. The lower plate displays four holes for Φ20 mm ground fixation bolts. Some additional Φ30 mm holes in the upper plate, as well as side openings, allow for a sufficient space for the bolt nut and optional washer to be set up when affixing the connector. Indeed the bolts are typically anchor bolts cast in a concrete foundation. The upper cross-shaped part of the connector is formed of 200 mm-high 6 mm-thick metal "wings" designed to be slotted inside the lower end of the timber column. The connection with the column is achieved using four Φ16 mm metallic pins disposed perpendicularly in two groups, respectively 20 mm and 50 mm away from the top of the connector. The total dimensions of the connectors are 170 mm × 170 mm × 240 mm.

The timber specimens used in the experimental tests are 800 mm-long Glulam beams with a cross-section of 180 mm × 180 mm. The specimen are made of Japanese larch (Larix kaempferi), the most common wood species for construction in Korea. The lower 200 mm part of the timber member is affixed to the metallic connector described above, while the upper part is affixed to an oil jack disposed horizontally in order to apply a moment to the joint (Fig. 3). The load is applied through loading metal plates on both sides of the specimen, allowing for reversed loadings. The pseudo-static loading is based on the ISO-16670 protocol for mechanical timber joints tested under quasi-static reversed cyclic loading [14]. It is composed of series of 3 cycles at constant amplitude, each series having an increasing amplitude of 1, 5, 10, 20, 40, 60, and 80 mm. Loading speed in set to 1 mm/s, which is a medium value in the range allowed by ISO-16670 (0.1 mm/s to 10 mm/s). This allows keeping the complete test within 30 minutes while avoiding
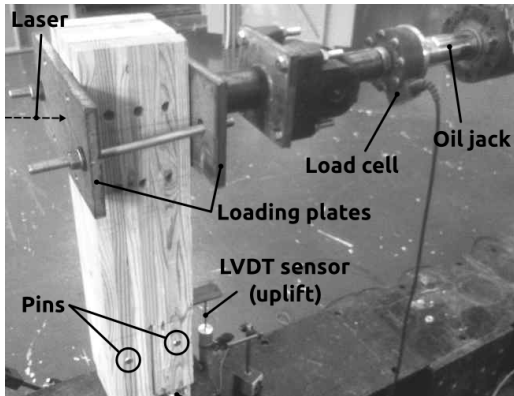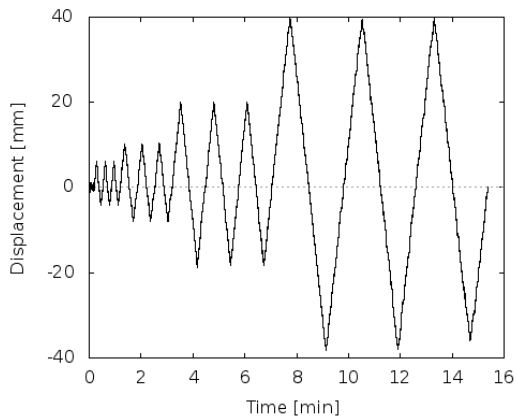
Fig. 3. Experimental device for moment test.

Fig. 4. Displacement load according to ISO 16670.

possible dynamic effects at high speed. An example of the actual loading as recorded by an external sensor during one of the experiments is shown on Fig. 4. In this particular test, the experiment was stopped after the complete damaging of the connector following the cyclic series of 40 mm lateral displacement amplitude (0.057 rad, or 3.3 degrees).

The tests are recorded using several internal and external sensors. A LVDT displacement sensor is affixed near the base of the specimen to measure the vertical uplift (Fig. 3). The load is measured using an internal 100 kN load cell. A laser displacement sensor aligned with the oil

jack and disposed on the other side of the specimen measures the actual horizontal displacement at the top of the timber member. The height of the laser beam and the axis of the oil jack with respect to the connector base is 700 mm. The tests are repeated to limit experimental discrepancies in results.

3. EXPERIMENTAL RESULTS

The evolution of the rotation of the joint function of the moment is presented in Fig. 5. This evolution is typical of timber joints with metallic connectors undergoing reversed loadings, where the nonlinear effects of damaging of the joint through plasticizing of the connector produce hysteresis loops. The equivalent linear rotational stiffness is roughly equal to 400 kN・m /rad. However, we can observe a pinching area around the origin with a lower stiffness due to the previous damaging of the metal connector. The initial linear elastic rotational stiffness, taken without the slip effect, is therefore higher, around 460 kN・m/rad. The moment resistance of the joint is around 11 kN・m in one direction and 8 kN/m in the opposite direction, for a rotation at failure of 0.029 rad (1.6 °). The asymmetry of the results is likely due to an error in the experimental setup which was corrected in the second test series (see below).

The failure of the joint occurs in the metallic connector only (Fig. 6). No timber damage is observed. The failure is characterized by a breaking of the welding between the lower and upper horizontal metal plates which compose the base of the connector. More precisely, the welding located on the traction side perpendicular to the rotation axis and on the lower face of the upper plate exhibit the earliest failure. On the compression side, the area of contact is much larger, corresponding to half of the cross-shaped cross-section. But, on the traction side, stresses are un-
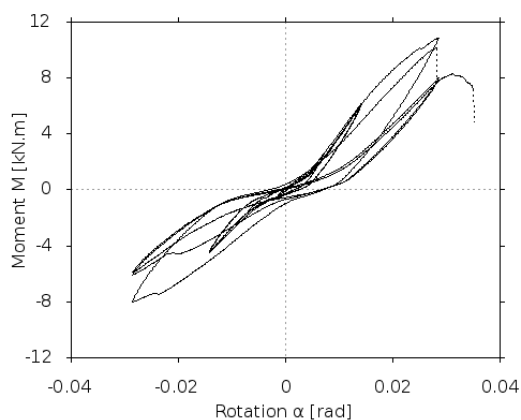
Fig. 5. Moment-rotation evolution in the joint in the original configuration.
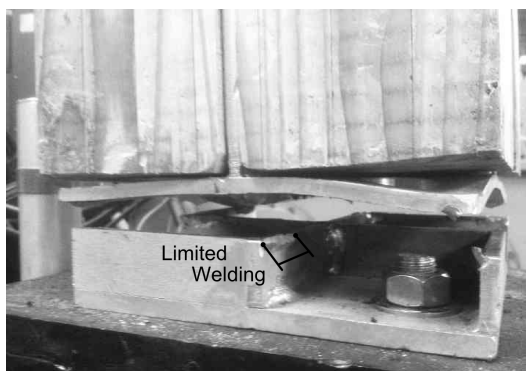

Fig. 6. Failure of the metallic connector in the weldings.

dergone by weldings only. Whereas on the upper face of the upper plate the weldings are continuous over the full contact surface between the vertical wings and the upper plate, as seen on Fig. 2, on the lower face weldings are located at discrete spots only, one of which is clearly visible after failure on Fig. 6. This configuration produces stress concentrations those weldings of limited length (2 cm), resulting in their failure. This result is confirmed later with the numerical simulation results (see below).

A failure in the metallic connector rather than in the wood is usually considered resulting from

a good design, and a desired behavior regarding safety, because it replaces the sudden brittle fracture of wood with the much slower plasticizing of metal while allowing for energy dissipation. Preventing a brittle fracture allows for longer evacuation delays in case of emergency and approximate visual prediction of the collapse time, while energy dissipation is of particular interest for seismic concerns. However in the present case we can notice that this dissipation is not very high under moment loading, producing hysteresis loops with a rather moderate thickness. This is due again to the limited length of the welding spots and their relative weakness as compared to the constitutive material of the connector.

In order to quantify this qualitative result, we introduce two quantities. First, the method proposed in [15] is used, which aims at quantifying the cyclic performance of shearwalls. Because the hysteresis behavior of the joint is similar to those of a shearwall, only at a different scale, we apply this method for quantifying the ductility and energy dissipation of the joint. The method introduces an equivalent energy elastic-plastic (EEEP) curve, defined by a yield limit a_v, and an ultimate limit a_u and associated moment M_u (Fig. 7). The values of a_u is the experimental rotation angle at failure ($a_u = 0.029$ rad). The elastic rotational stiffness of the EEEP curve, that is M_u/a_v, is equal to the elastic rotational stiffness derived from the experimental data. Because the joint exhibits a progressive nonlinear behavior, as opposed to two distinct elastic and plastic phases, it is difficult to clearly determine the yield point on the experimental curve. Therefore, we use the tangent stiffness between 10% and 40% of the peak moment M_{max}, as proposed by the Japanese method. This gives us an elastic rotational stiffness of 457 kN・m/rad. The value of M_u is then derived based on the assumption of equivalent energy dissipation
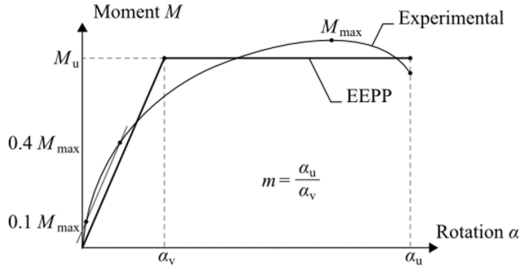
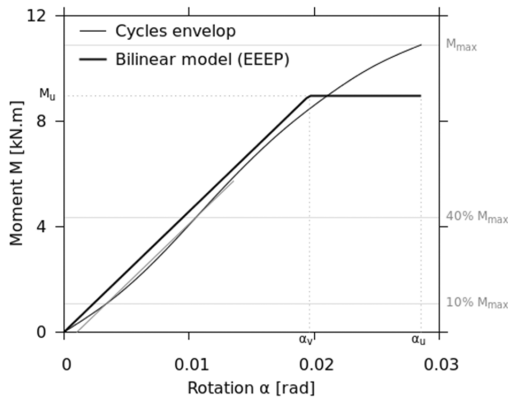Fig. 7. Equivalent bilinear model using the method described in [15].

Fig. 8. Energy equivalent elastic plastic (EEEP) bilinear model using the method described in [15].

between the EEEP model and the experimental data (equal areas). We obtain $M_u = 8.96$ kN・m. The yield limit $a_v = 0.020$ rad is then simply obtained using M_u and the elastic rotational stiffness. The resulting EEEP model is presented in Fig. 8.

The method defines a ductility ratio m as the ratio a_u/a_v. This ratio quantifies the capacity of the system to undergo plastic deformations; the limit m = 1 corresponds to an elastic brittle behavior, while m increases with more ductile behavior. In this case, we obtain a ductility ratio m = 1.46, which characterizes a low ductility system. The Japanese design code defines a structural characteristic factor D_s quantifying the strength reduction under plastic deformation as

compared to an ideal linear elastic behavior. This quantity is related to energy dissipation plasticizing: lower values of D_s correspond to a greater strength reduction, and therefore a greater dissipated energy. The lower limit for design is $D_s = 0.25$; conversely a value of $D_s = 1$ corresponds to an elastic-brittle system. The inverse of this coefficient ($1/D_s$) is similar to the behavior factor q of the European design codes [16, 17], which aims at taking into account the strength limitation under plastic deformation in a seismic analysis. A comparison of the few details between those coefficients is available in [18]. Although D_s and q are design parameters, that is they should be derived from characteristic values using safety coefficients, we can anyway compute a similar "experimental" D_s from experimental data as a mean of comparison to quantify the joint improvement (see below). For the sake of simplicity we use the same notation. Therefore D_s is computed as the ratio of the experimental maximum strength M_{max} at failure over the strength at failure Mel for a hypothetical linear elastic behavior. The linear elastic rotational stiffness is derived from the EEEP model, and we obtain Mel = 12.4 kN・m/rad. It comes $D_s = 0.88$. This is close to the brittle behavior limit ($D_s = 1$), thereby confirming the low ductility and low energy dissipation of the joint. In the literature, the analytical relation $D_s = 1/\sqrt{(2m-1)}$ is sometimes used. This corresponds to a value of D_s derived from an elastic-perfectly plastic curve like the EEEP model, and thus using M_u instead of M_{max}. Using this relation, we obtain an approximated $D_{s,\ EEP} = 0.72$, which slightly overestimate the real strength reduction. Obviously, this overestimation is inherent to the perfectly plastic behavior which produces an ultimate moment lower than the experimental value ($M_u < M_{max}$).

Concerning the uplift, the measured values of the vertical displacement as reported by the LVDT

sensor are approximately in the range of ±5 mm. However, due to the experimental setup these values originate mostly from the rotation of the timber member itself. After correction of this effect, we obtain a negligible value for the real uplift, that is the differential displacement between the connector and the timber column. Postest observations show that the metal pins are undamaged, which confirm this result.

In conclusion of those experimental tests, the failure of the joint in the metal connector is obtained as expected from a careful design of a timber joint with a metallic connector. However, considering a scenario of horizontal reversed loading (*e.g.* an earthquake), the ductility and energy dissipation are found to be rather low because the failure occurs in the connector weldings rather than around the pins.

4. NUMERICAL STUDY

In order to complement the experimental results, we perform a numerical study with a very refined finite element (FE) model.

4.1. Numerical model

The model of the joint is presented in Fig. 9. The mesh is composed of approximately 10^5 second-order volume elements (20-node hexahedra and 10-node tetrahedra) with a size ranging from 50 mm in areas of less interest down to 1 mm in areas of concentrated stresses, *i.e.* typically around pin holes and weldings. We perform static nonlinear simulations. The nonlinearities arise from the presence of contact only.

The material parameters of the FE model are summarized in Table 1. The wood is modeled using a linear elastic orthotropic material with a density ρ_w of 520 kg/m^3 and an elasticity modulus E_{wL} of 14.2 GPa in the longitudinal direction (along the column long side, vertically).
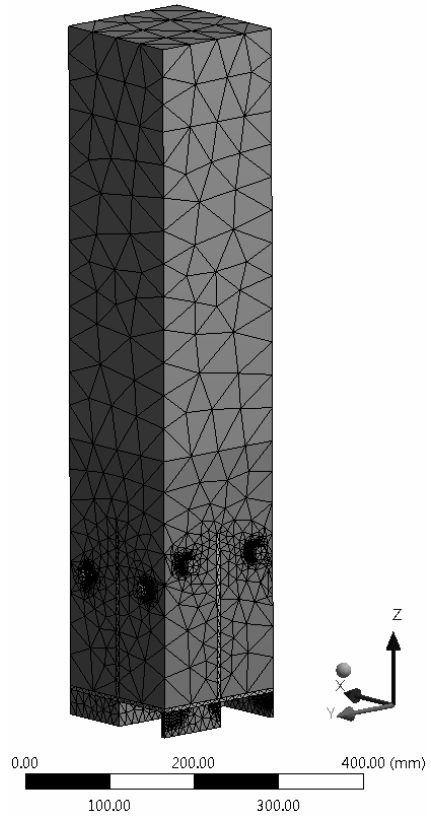

Fig. 9. Mesh of the refined finite element model.

Table 1. Finite element model parameters

Material	Parameter	Value
Wood	Density	$\rho_w = 5203$ kg/m^3
	Elasticity modulus (L)	$E_{wL} = 14.2$ GPa
	Elasticity modulus (T)	$E_{wT} = 1$ GPa
Steel	Density	$\rho_s = 78503$ g/m^3
	Elasticity modulus	$E_s = 210$ GPa

The tangential modulus of elasticity E_{wT} is taken equal to 1 GPa. Those parameters correspond to a larch species as reported in [19]. The steel of the connector and the pins is modeled with a linear elastic isotropic material with a density ρ_s of 7,850 kg/m^3 and an elasticity modulus E_s of 210 GPa.

Concerning the boundary conditions of the model, the base of the connector is fixed, while the load is applied on the upper part of the wood member on an area of 100 mm height (0.018 m^2) roughly equal to the size of the loading metal plates used in the experimental tests. Contact is set between the wood and the metal the connector to allow for relative slip along the connector wings and uplift from the horizontal base.

4.2. Numerical Results

The maximum stress in the steel is reached in the base of the connector at the junction between the horizontal upper plate and the vertical cross-shaped support beneath it (Fig. 10). This qualitative result is consistent with the experimental tests, since this is precisely the location of the experimental failure. The numerical results given by the FE method are computed using linear elastic materials. Therefore, the materials do not have any strain or stress limit during the simulation. As a result, additional criteria must be verified *a posteriori* to ensure physical consistency. We take a reference embedding strength of wood f_h = 35 MPa for a load parallel to wood grain [20], and a tensile strength perpendicular to wood grain of 3 MPa [19]. For the steel of the connector and the pins, we consider an ultimate strength $\sigma_{s,u}$ = 460 MPa. Those parameters are summarized in Table 2. The ultimate strength of steel $\sigma_{s,u}$ is reached for an input load around 10 kN. This value is consistent with the experimental results. Fig. 10 also underlines the stress concentrations around the pin holes in the metallic connector. However the maximum stress remains below the ultimate strength, so no wood failure or pin damage occur.
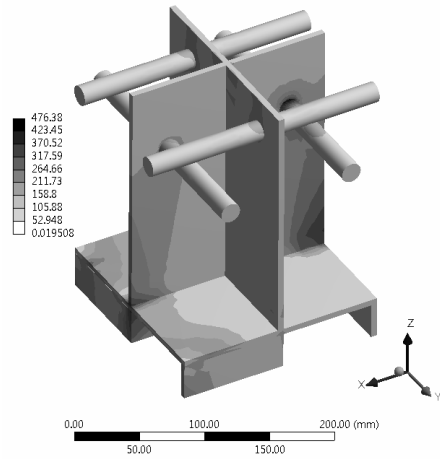

Fig. 10. Stress (in MPa) in the connector and the pins for an input lateral load of F = 10 kN.

Table 2. Post-processing material limits

Material	Parameter	Value
Wood	Embedding strength	f_h = 35 MPa
	Tensile strength	f_t = 3 MPa
Steel	Ultimate strength	$\sigma_{s,u}$ = 460 MPa

5. IMPROVING THE CONNECTOR

Following these results, we aimed at improving the ductility and energy dissipation of the joint by increasing the resistance of the weldings. In an effort to make the slightest changes, we decided to cut the lower end of the timber member to allow directly bolting the upper plate of the connector and prevent the failure shown on Fig. 6. Indeed the weldings of the upper plate with the "wings" are continuous all along the borders, as seen on the undamaged connector of Fig. 2, and were therefore expected to be much more resistant. The resulting assembly is presented in Fig. 11.

A second series of experimental tests is then conducted using this configuration, all experimental setups being equal otherwise (*i.e.* including the same reversed cyclic loading). The evo-

Fig. 11. Direct bolting of the connector upper plate.

Fig. 13. Equivalent bilinear model of the results on the improved connector using the method from [15].
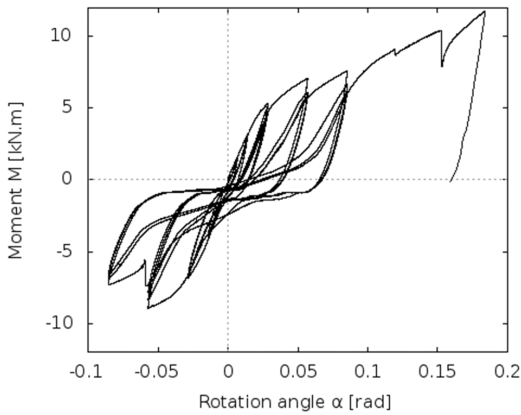

Fig. 12. Moment-rotation evolution in the joint when bolting directly the top plate of the connector.

lution of the moment function of the rotation angle at the base of the connector is presented in Fig. 12 for this new configuration. The resistance of the connector is the same as in the first series, around 11 kN・m. However the ductility has been much improved, as the maximum rotation angle at failure a_u reaches 0.184 rad (10.5 degrees). As previously, using the method described in [15] we derive an approximated bilinear EEEP model as shown in Fig. 13. With this configuration, we obtain an ultimate moment M_u = 9.06 kN・m very close from the one obtained in the initial configuration (8.96 kN・m). The equivalent elastic rotational stiffness of this bilinear model is 198 kN・m/rad. It

is much lower than in the initial configuration because of the increased rotation yield limit a_v = 0.046 rad. Globally, we see that the resistance is approximately the same, while the rotations are much higher. As earlier, we compute the ductility factor m and the energy dissipation factor D_s. The obtained values are m = 4.02 and D_s = 0.49. The increase of m and decrease of D_s both confirm that the ductility and energy dissipation of the joint in this configuration are improved as compared to the initial configuration, while retaining a same resistance. The approximated structural factor based on the EEEP model is $D_{s,\ EEEP}$ = 0.38. The comparison is summarized in Table 3. The direct bolting of the upper metal plate of the connector delayed the failure of the weldings and greatly improved the ductility of the joint by allowing a greater plasticizing of the connector before failure. Cutting the lower end of the timber member allowed for larger displacements, which at the same time lowered the initial elastic rotational stiffness of the joint. In the end, this practical modification of the configuration allows for a safer joint with higher ductility and energy dissipation.

Table 3. Comparison of the performance of the joint in the original and improved configurations

Joint configuration	Strength M_{max} [kN·m]	EEEP limit M_u [kN·m]	EEEP stiffness [kN·m/rad]	Ductility factor m [-]	Structural factor D_s [-]
Original configuration	10.9	8.96	457	1.46	0.88
Improved configuration	11.8	9.06	198	4.02	0.49

6. CONCLUSIONS and PERSPECTIVES

We performed several experimental tests and numerical analyses on a recently developed design of timber column joint with a slotted-in metallic connector. This joint aims at replacing the traditional wood-wood joint found in the traditional Korean timber house (*Hanok*). The results of the experimental tests show a hysteresis behavior typical of timber joints with metallic connectors. This behavior allows the joint to dissipate energy through mechanical damaging of the metal parts, and provides an increased ductility over the traditional wood-wood connection used in *Hanok*. Therefore an increased safety is ensured as compared to a brittle wood fracture.

Experimentally, the failure of the joint under moment loading occurs as intended in the metallic connector. However, because this failure occurs in the weldings, the ductility remains limited in its original configuration, and therefore the failure is still considered too sudden when considering *e.g.* a seismic scenario. So in a second part we attempt to improve this point by improving the connector itself. We therefore modify the configuration of the connector to delay the welding failure observed experimentally. Results display a much higher ductility and energy dissipation while retaining a same level of rotational strength. The failure rotation angle increases from an initial 0.02 rad to more than 0.15 rad, the later being deemed suitable to withstand the ty-

pical displacements undergone by a 2.4 m tall shearwall undergoing a seismic loading corresponding to a low to moderate seismicity area like Korea.

Following these results, a next objective could be to improve the aesthetic of the joint by decreasing its visibility. A possible solution would be to obtain a failure in the metal pins, as it is typically the case in pinned connections, while preventing a brittle wood fracture and a welding failure. This is believed to be possible by using continuous weldings everywhere in the connector. The present solution is however considered satisfying given its limited visibility. Moreover, due to other requirements for timber structures (*e.g.* ground humidity insulation) a fully hidden column base joint connector is difficult to design. Regarding the numerical simulations, a macro-scale numerical model based on those results is being developed for use in subsequent simulations of a full-scale timber house, which should provide similar results at a much lower computation cost. Finally, uplift tension tests and shaking-table tests should provide complementary results on the behavior of these connectors and their interaction when included in a full-scale timber structure.

REFERENCES

1. Park. M. J. *et al.* 2010. Shear performance of hybrid post and beam wall system with structural insulation panel infill, in Proceedings of the 11th World Conference on Timber Engine-

ering, paper 456.

2. Komatsu. K. *et al.* 1998. Glulam Semi-Rigid Portal Frames Composed of Hardwood Wedges and Metal Wares, in Proceedings of the 5th World Conference on Timber Engineering.

3. Nakatani. M. *et al.* 2006. Development of mo-mentesisting joint systems using lagscrewbolts, in Proceedings of the 9th World Conference on Timber Engineering.

4. Buchanan. A. *et al. 2001.* Ductile moment-resisting connections in glulam beams, in Proceedings of the NZSEE conference.

5. A. Iqbal *et al.* 2005. Seismic Performance of Prestressed Timber Beam-Column Sub-Assemblies, in Proceedings of the NZSEE conference.

6. M. Noguchi *et al.* 2006. Development of wooden portal frame structures with improved columns, J. Wood Sci. 52: 51～57.

7. M. Newcombe, 2008. Seismic Design of Multi-storey Post-Tensioned Timber Buildings, Master Thesis, University of Pavia, Italy.

8. T. Smith, 2008. Feasibility of Multi Storey Post-Tensioned Timber Buildings: Detailing, Cost and Construction, Master Thesis, University of Canterbury.

9. N. Richard *et al.* 2003. Prediction of seismic behavior of wood-framed shear walls with openings by pseudodynamic test and FE model, J. Wood Sci. 49: 145～151.

10. M. Yasumura *et al.* 2006. Pseudodynamic tests and earthquake response analysis of timber structures II: two-level conventional wooden structures with plywood sheathed shear walls, J. Wood. Sci. 52(1): 69～74.

11. J. van de Lindt *et al.* 2011) Shake table testing of a full-scale seven-story steel-wood apartment building, Engineering Structures 33: 757～766.

12. K. Hwang *et al.* 2007. Shear performance of post and beam construction by pre-cut process, Mokchae Konghak 35(6): 1～12.

13. J. Humbert, 2010. Characterization of the Behavior of Timber Structures with Metal Fasteners Undergoing Seismic Loadings, Ph.D. Thesis, University of Grenoble, France.

14. International Organization for Standardization, 2003. ISO 16670: Timber Structures-Joints made with mechanical fasteners-Quasi-static reversed-cyclic test method, Geneva, Switzerland.

15. Architectural Institute of Japan, 2002. New estimation method for shear wall performance. Standard for Structural Design of Timber Structure (in Japanese), 104pp.

16. CEN, 2004. Eurocode 5-Design of Timber Structures, EN 1995.

17. CEN, 2004. Eurocode 8-Design of Structures for Earthquake Resistance, EN 1998.

18. E. M. Marino, M. Nakashima, and K. M. Mosalam, 2005. Comparison of European and Japanese seismic design of steel building structures, Engineering Structures 27: 827～840.

19. D. Kretschmann, 2010. Wood Handbook. Chapter 05: Mechanical Properties of Wood, Technical Report FPL-GTR-190.

20. K. Sawata and M. Yasumura. 2002. Determination of embedding strength of wood for dowel-type fasteners, J. Wood Sci. 48: 138～146.